Comprehensive Computational Profiling of Some New Candidate Molecules for Huntington's Disease: Drug-Likeness, Quantum Descriptors, Molecular Docking, Molecular Dynamics Simulation and Synthetic Mechanism

F. Islamoglu*

Department of Chemistry, Faculty of Science and Arts, Recep Tayyip Erdogan University, 53100, Rize, Türkiye

fatih.islamoglu@erdogan.edu.tr

Keywords: *Huntington's disease, Computational drug design, Quantum chemical descriptors, Molecular docking and Molecular dynamics simulation.*

In this study, the potential use of five novel 5,10-dihydrochromeno[5,4,3-cde]chromene-5,10-diol derivatives, which have never been synthesized before and are not reported in the literature, as active pharmaceutical ingredients for the treatment of Huntington's disease was investigated. Huntington's disease is a hereditary neurodegenerative disorder that causes progressive loss of nerve cells. Firstly, Boiled Egg graphs for molecular gastrointestinal (GI) absorption and blood-brain barrier (BBB) permeability and bioavailability radars for understanding the oral bioavailability suitability of molecules were generated. Then, molecular docking studies were conducted using AutoDock Vina software to predict the binding potential of molecules to biological targets, analyze interactions, and guide experimental stages in the drug discovery process against five different Homo sapiens proteins with resolution values ranging from 2.84 Å to 2.97 Å. The highest molecular docking result was obtained as 11.4 kcal/mol, a result of the interaction between 2,7-diethyl-3,8-dimethyl-5,10-dihydrochromeno[5,4,3-cde]chromene-5,10-diol (3) and the protein with PDB ID code 8T69. To further elucidate the structural and electronic features of the most promising candidate, highest occupied molecular orbital energy (E_{HOMO}: -0.337 a.u), lowest unoccupied molecular orbital energy (E_{LUMO}: 0.255 a.u), chemical potential (μ: 0.061 a.u), electron affinity (EA: -0.255 a.u), global softness (S: 1.582 a.u), global hardness (η: 0.316 a.u), ionization potential (IP: 0.377 a.u), total energy (SCF: -70.301 a.u), dipole moments (1.669 debye), electrophilicity index (ω: 0.005887658 a.u), bond angles, bond lengths, Mulliken atomic charges, and molecular electrostatic potential (MEP) were analyzed. Molecular dynamics simulations were performed to predict large-scale conformational changes. Finally, a reaction mechanism for the synthesis of the lead molecule has been proposed.

Introduction

Huntington's disease is an autosomal dominantly inherited neurodegenerative disorder characterized by chorea, cognitive impairment, and psychiatric symptoms due to an increase in cytosine, adenine, and guanine repeats in the short arm of the Huntingtin gene located at chromosome 4p16 [1]. The most common psychiatric symptoms seen in this weekly report are depression, anxiety disorder, obsessive-compulsive disorder, and psychosis. Cognitive impairment, one of the main symptoms of the disease, may also be seen before the motor stage, or it may be mild in some patients with advanced motor and psychiatric findings [2]. The main cause of dysphagia in Huntington's disease is a combination of hyperkinetic and, less frequently, hypokinetic disorders seen not only in the extremities but also in the oropharyngeal muscles. Unpredictable and rapid tongue and buccal muscle movements cause food to enter the pharynx [3]. There is currently no approved disease-modifying treatment for Huntington's disease, and symptomatic treatments are used to try to control the clinical course [4].

Tetrabenazine, a vesicular monoamine transporter 2 inhibitor used in the treatment of chorea associated with Huntington's disease and tardive dyskinesia, is a second-generation tienobenzodiazepine that inhibits the uptake of certain chemicals (such as dopamine and serotonin) in the central nervous system (CNS) and reduces dopamine transport to decrease involuntary movements [5], deutetrabenazine, a vesicular monoamine transporter 2 inhibitor used in the treatment of chorea associated with Huntington's disease and tardive dyskinesia [6], Olanzapine, a second-generation antipsychotic agent from the thienobenzo-diazepine class, is a nonspecific inhibitor of multiple 5HT, dopamine, and muscarinic receptors, and its binding to dopamine-2 receptors is responsible for its antiemetic benefit [7], and Risperidone, which is indicated for monotherapy or combination therapy in the treatment of schizophrenia and acute manic or mixed episodes of bipolar disorder in adults [8].

In this study, we investigated five different 5,10-dihydrochromeno[5,4,3-cde] chromene-5,10-diol derivative molecules, which have not been synthesized before and are not recorded in the literature, for their potential use in the treatment of Huntington's disease by interacting with five different synaptic vesicular amine transporters (VMAT) found in neurons and neuroendocrine cells, which are carrier proteins responsible for pumping neurotransmitter amines (dopamine, serotonin, norepinephrine, and histamine) and facilitating their storage. Based on this point, the aim of this study is to investigate the potential use of 5,10-dihydrochromeno[5,4,3-cde]chromene-5,10-diol derivative molecules, which have not been synthesized before and

are not found in the literature, as drug active ingredients in the treatment of Huntington's disease using the molecular docking method. Computer-assisted studies are of great importance today and make significant contributions to the literature [9-12]. Researchers have demonstrated that molecular docking and molecular dynamics simulation play a significant role in the development of new drug active ingredients [13-16].

Materials and method

Molecules

In this study, five different 5,10-dihydrochromeno[5,4,3-cde]chromene-5,10-diol derivatives (2,7-dimethyl-5,10-dihydro chromeno[5,4,3-cde]chromene-5,10-diol **(1)**, 2,3,7,8-tetramethyl-5,10-dihydrochromeno[5, 4,3-cde]chromene-5,10-diol **(2)**, 2,7-diethyl-3, 8-dimethyl-5,10-dihydrochromeno[5,4,3-cde] chromene-5,10-diol **(3)**, 2,3,7,8-tetraethyl-5, 10-dihydrochromeno[5,4,3-cde]chromene-5, 10-diol **(4)**, 2,7-diethoxy-3,8-di methyl-5,10-dihydrochromeno[5,4,3-cde]chromene-5,10-diol (5)) were examined. The molecular formulas of these molecules are given in **Figure 1**.

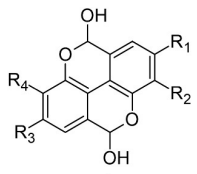

Molecule	R_1	R_2	R_3	R_4
1	$—CH_3$	—H	$—CH_3$	—H
2	$—CH_3$	$—CH_3$	$—CH_3$	$—CH_3$
3	$—CH_2CH_3$	$—CH_3$	$—CH_2CH_3$	$—CH_3$
4	$—CH_2CH_3$	$—CH_2CH_3$	$—CH_2CH_3$	$—CH_2CH_3$
5	$—OCH_2CH_3$	$—CH_3$	$—OCH_2CH_3$	$—CH_3$

Figure 1. Molecular formulas of the 5,10-dihydro chromeno[5,4,3-cde] chromene-5,10-diol derivatives

Brain/Intestinal estimated permeation method

For a drug to be developed for a neurodegenerative disease such as Huntington's disease, the ability of the active ingredient to cross the blood-brain barrier (BBB) is of vital importance and, in most cases, is essential. Therefore, to determine whether the molecules we are examining here can cross the blood-brain barrier, BOILED-Egg graphs were created using the SwissADME [17] website. BOILED-Egg positions molecules on two axes. These are WLOGP (indicates the lipophilicity (logP) of the molecule) and TPSA (topological polar surface area, indicates the polar surface area of the molecule). If the molecule is in the egg white region of the graph, it indicates a high likelihood of good absorption in the gastrointestinal system and high oral bioavailability. If the molecule is in the yolk region, it likely indicates that it can cross the blood-brain barrier. Generally, drug candidates targeting the central nervous system are found in this region. If molecules are outside these two regions, it indicates a risk of both poor oral absorption and poor BBB penetration. The resulting graph is shown in **Figure 2**.

Bioavailability radar

Bioavailability radar is a graph drawn to quickly and multidimensionally evaluate the pharmaceutical suitability (drug-likeness) of a

molecule. It is possible to create these graphs through various websites.

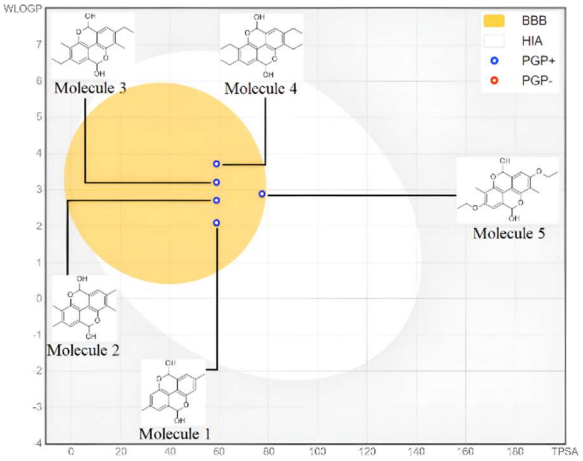

Figure 2. BOILED-Egg graph for molecules

In this study, bioavailability radars were created for all molecules using the SwissADME (http://www.swissadme.ch/) [17], which creates this radar based on six different parameters such as LIPO (lipophilicity), SIZE (molecular weight), POLAR (topological polar surface area), INSOLU (solubility in water), INSATU (unsaturation, sp3 ratio), and FLEX (number of rotatable bonds), and the ADMETLab3.0 database (https://admetlab3. scbdd.com/) [18] probabilities with values between 0 and 1 were the output value. Sensitivity was denoted by category 1, and non-sensitivity by category 0. The projected data that resulted was downloaded for additional examination. ADMETLab3.0 database, which creates this radar based on thirteen different parameters such as MW (molecular weight), nRig (number of rigid bonds), fChar (formal charge), nHet (number of heteroatoms), MaxRing (maximum ring size), nRing (number of rings), nRot (number of rotatable bonds), TPSA (topological polar surface area), nHD (number of hydrogen donors), nHA (number of hydrogen acceptors), logD (distribution coefficient), logS (aqueous solubility), and logP (partition coefficient, octanol/water). All radars obtained for the molecules are given in **Figure 3**.

Ligand preparation and optimization

The 3D structures of the five different 5,10-dihydrochromeno[5,4,3-cde]chromene-5,10-diol derivatives were drawn and energy minimized using Chem3D software [19]. For future research, the optimized ligands were stored in pdbqt format.

Protein preparation and molecular docking

Using Discovery Studio software [20], the receptor molecule was prepared before docking by eliminating extraneous components from the crystal structures, such as water, heteroatoms, and hydrogen bonds. The X-ray crystallographic structure of five synaptic vesicular amine transporters as targets in Homo sapiens was downloaded from the Protein Data Bank (PDB ID (resolution): 8JSW (2.84 Å), 8T69 (2.89 Å), 8WRE (2.90 Å), 8JTB (2.93 Å), 8JT9 (2.97 Å). The chain number and active site residues of each PDB protein have been determined, and the coordinates according to which the docking box is set and the active site it covers are clearly specified. AutoDock Vina [21, 22] was used to do molecular docking. I have

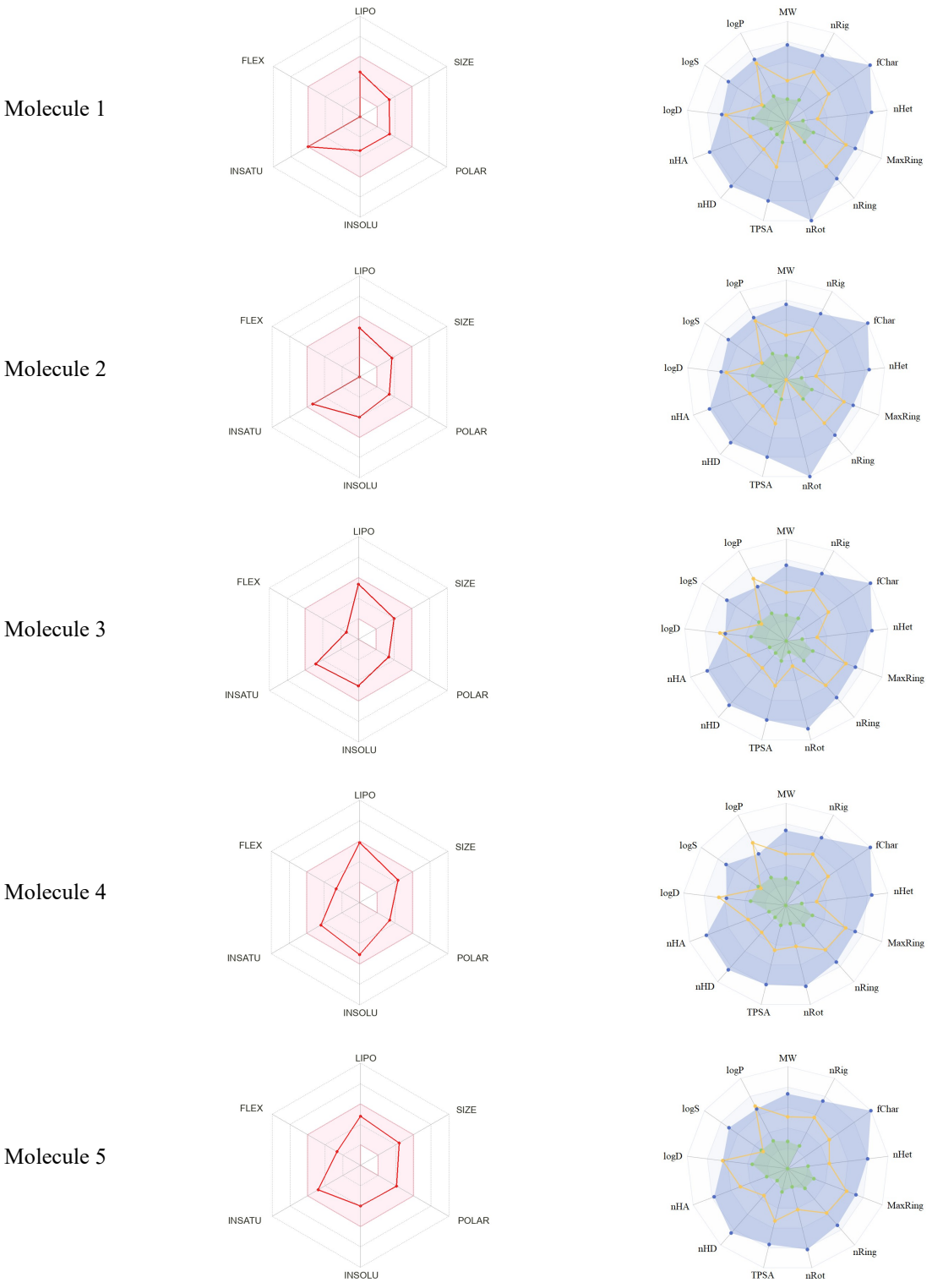

Figure 3. Bioavailability radars drawn for all molecules using the SwissADME and ADMETLab3.0 websites

included docking protocol validation. Re-docking of co-crystallized ligands was performed, and RMSD values between experimental and docked poses were found to be <2.0 Å, indicating reliable docking accuracy. Furthermore, ROC curve analysis was conducted, showing AUC values >0.80, which supports the robustness of the docking

method. The Discovery Studio software [20] was used to visualize the resultant with a higher binding affinity (kcal/mol). Results were obtained for five different modes for each molecule. The results are seen to be in the range of 11.4 – 4.7 kcal/mol. The highest binding affinity (11.4 kcal/mol) was obtained as a result of the interaction between 2,7-diethyl-3,8-dimethyl-5,10-dihydrochromeno [5,4,3-cde]chromene-5,10-diol **(3)** and the protein with PDB ID code 8T69. The molecular docking results obtained are given in **Table 1**.

Table 1. The obtained molecular docking results

Molecule	PDB Code	Affinity (kcal/mol)				
		Mode 1	Mode 2	Mode 3	Mode 4	Mode 5
1	8JSW	-8.30	-6.80	-6.60	-6.30	-6.20
	8T69	-11.30	-6.20	-6.10	-6.00	-5.70
	8WRE	-8.90	-7.80	-7.80	-7.50	-6.20
	8JTB	-9.10	-7.00	-6.70	-6.30	-6.00
	8JT9	-10.40	-6.80	-6.70	-5.10	-5.10
2	8JSW	-8.90	-6.90	-6.60	-6.40	-5.80
	8T69	-10.20	-6.50	-6.20	-6.20	-5.70
	8WRE	-9.10	-7.70	-7.50	-7.40	-6.30
	8JTB	-9.90	-6.90	-6.80	-6.70	-6.50
	8JT9	-10.50	-7.20	-7.00	-5.50	-5.30
3	8JSW	-8.80	-6.70	-6.60	-6.40	-6.20
	8T69	-11.40	-6.30	-6.10	-6.10	-6.00
	8WRE	-9.10	-7.60	-7.50	-6.50	-6.20
	8JTB	-9.50	-7.20	-6.80	-6.50	-6.50
	8JT9	-9.90	-7.20	-6.40	-5.90	-5.40
4	8JSW	-8.70	-6.30	-6.30	-6.20	-5.40
	8T69	-10.90	-6.30	-6.10	-5.90	-5.70
	8WRE	-9.10	-7.20	-6.90	-6.90	-5.70
	8JTB	-8.90	-7.00	-6.70	-6.50	-6.50
	8JT9	-10.20	-6.90	-6.30	-5.50	-5.40
5	8JSW	-8.10	-6.60	-6.40	-6.30	-5.60
	8T69	-9.70	-5.90	-5.80	-5.60	-5.40
	8WRE	-8.40	-7.10	-6.80	-6.10	-6.10
	8JTB	-8.90	-6.40	-6.40	-6.20	-6.10
	8JT9	-9.70	-6.50	-6.40	-5.10	-4.70

Ramachandran plots were drawn for the protein with PDB ID code 8T69, for which we obtained the highest docking score using the Ramplot [23]. The resulting Ramachandran plot-2D and Ramachandran plot-3D are shown in **Figure 4**. The stereochemical quality of the protein structure 8T69 was given Figure 4 was assessed using the Ramachandran plot. The majority of residues, 72.4% (278 residues), were located in the most favored right-handed α-helix region, while 6.8% (26 residues) occupied the β-sheet region. Glycine and proline residues, which are known to adopt atypical conformations due to their structural flexibility and cyclic nature, accounted for 9.6% (37 residues) and 4.9% (19 residues), respectively. Only 0.3% (1 residue) was observed in the left-handed α-helix region. Importantly, 6.0% (23 residues) fell into disallowed regions, which may indicate local conformational strain or regions requiring further refinement. Overall, these results

suggest that the structure is stereochemically reliable, with the majority of residues adopting energetically favorable conformations. The 2D and 3D visualizations of this interaction are given in **Figure 5**. A detailed visual representation of the interaction types and bond length distances in angstroms (Å) is given in **Figure 6**.

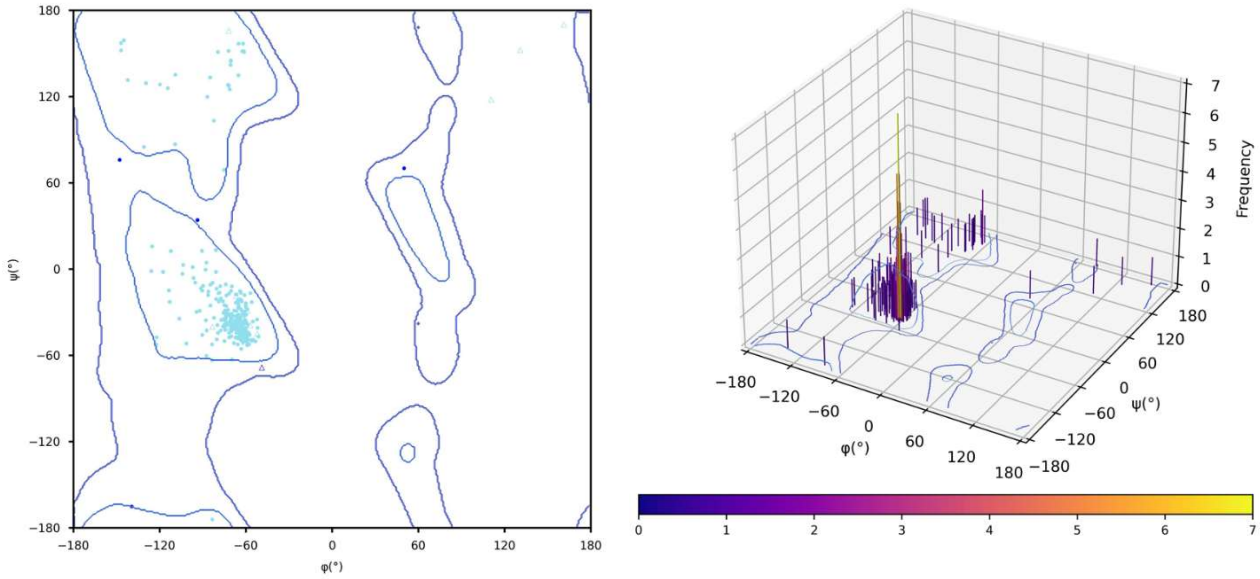

(a) (b)

Figure 4. Ramachandran plot-2D (a) and Ramachandran plot-3D (b) for PDB ID code 8T69

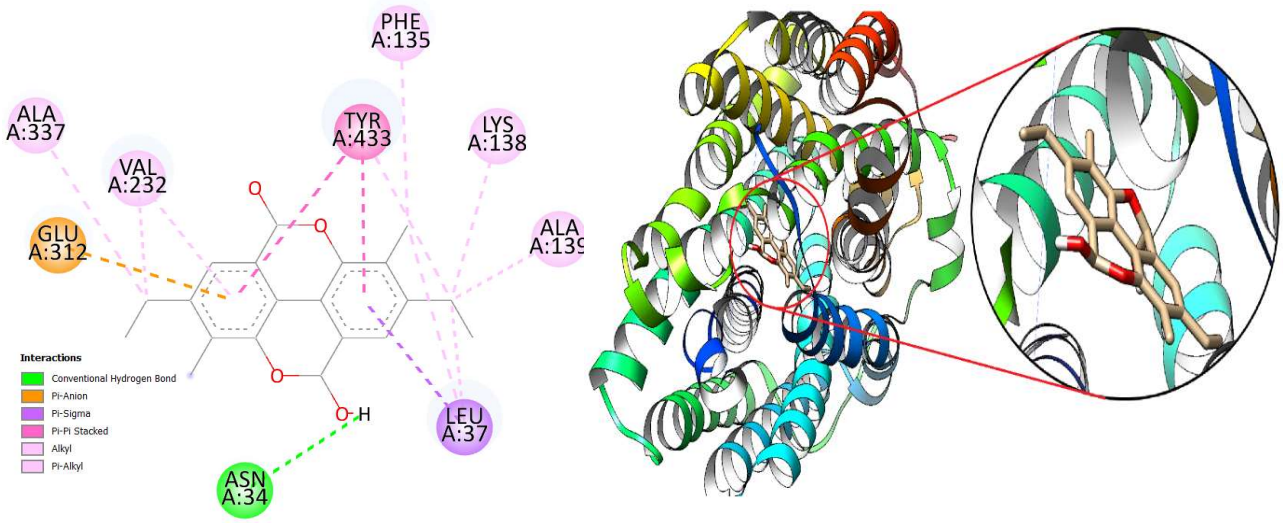

(a) (b)

Figure 5. 2D (a) and 3D (b) representation of ligand interaction with receptor residues

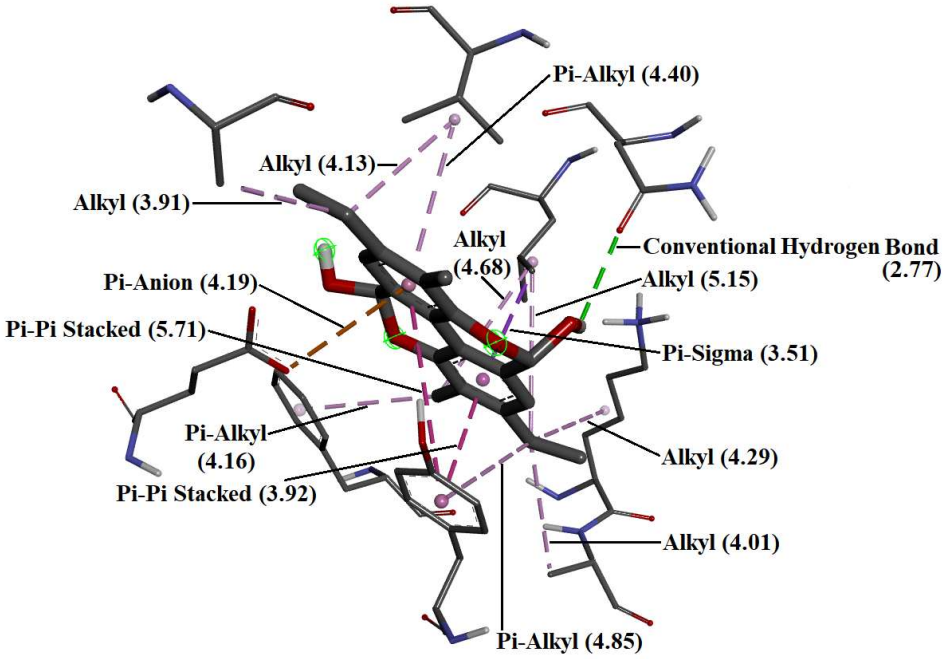

Figure 6. 3D representation of the interaction types and bond length distances (Å)

Molecular dynamics simulation

With the use of MD simulation, we can see at the atomic level how a molecule's atoms (such as a drug candidate) and their surrounding materials (proteins, solvents, and ions) change over time at particular pressures and temperatures [24]. It uses interatomic forces to mimic realistic movements and is based on Newtonian mechanics [25]. Furthermore, it goes beyond the static structure to evaluate the effects of mutations, reveal flexible regions and possible allosteric regions, test binding stability, identify important interactions, provide a basis for binding free energy calculations, and incorporate aqueous environment effects [26]. The Molecular dynamics simulation was performed using a web-based server called iMODS (Internal Coordinate Normal Mode Analysis Server, http://imods.chaconlab.org/) [27]. This method quickly analyzes the conformational flexibility and internal movements of in silico protein–ligand complexes. Classical MD simulation iteratively solves the motion over time using atom-atom force fields. iMODS, on the other hand, performs Normal Mode Analysis (NMA) and calculates the lowest-energy vibration modes to predict the molecule's natural movement tendencies [28].

Result and discussion

As a result of all our studies on the five different 5,10-dihydrochromeno[5,4,3-cde] chromene-5,10-diol derivatives I examined in this study, it was observed that all molecules can cross the blood-brain barrier (all molecules are within the yellow area), as shown in Figure 2. BOILED-Egg graph: all molecules were observed to be able to cross the blood-brain barrier (all molecules are within the yellow area). When examining the bioavailability radars shown in Figure 3, it is observed that all molecules are within the pink area in the

graphs obtained with SwissADME, indicating that all molecules can be considered as drug candidates. In the bioavailability radars obtained with ADMETLab3.0, only molecules 1 and 2 are within the purple area in the relevant graph, leading to the conclusion that only these two molecules are stronger as drug candidates, while the remaining molecules 3, 4, and 5 can be considered weaker.

When examining the molecular docking results given in Table 1, it can be seen that the highest score of 11.40 kcal/mol was obtained from the interaction of the third molecule with the protein PDB ID: 8T69. In this interaction, which yielded the highest docking score, a total of fourteen different chemical interactions of six different types were observed, classified as pi-alkyl (4.40, 4.85, 4.16), hydrogen bond (2.77), alkyl (5.15, 4.29, 4.01, 3.91, 4.13, 4.68), pi-sigma (3.51), pi-pi stacked (3.92, 5.71), and pi-anion (4.19). Based on the presence and distances of hydrogen bonds, I know from the literature [29] that molecular contact with 2.5 Å<d<3.1 Å indicates a strong interaction, while 3.1 Å<d<3.55 Å indicates a weak interaction. Based on this literature information, I can say that the interaction we observe in our molecule is a strong interaction in terms of hydrogen bonds. To better analyze this interaction, I examined it in terms of aromaticity, interpolated charge, H-bonds, hydrophobicity, ionizability, and SAS (solvent accessible surface area). The interaction images I obtained are given in **Figure 7**.

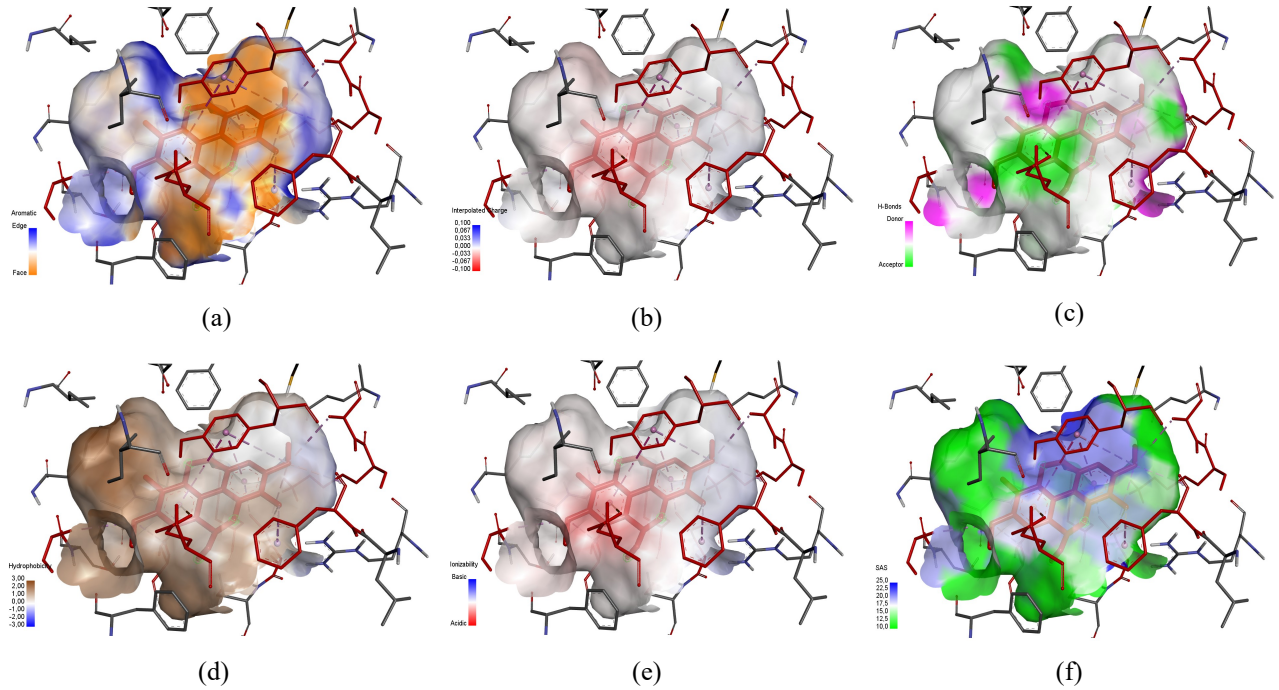

Figure 7. Three-dimensional aromaticity (a), interpolated charge (b), H-bonds (c), hydrophobicity (d), ionizability (e), and SAS (solvent accessible surface area) (e) structures of molecule **(3)**

The bond angles and bond lengths of a drug candidate are important, and this importance is twofold in terms of both structural stability and biological interaction [30]. Bond lengths and angles determine the molecule's lowest energy state, rigidity or flexibility, the positioning of functional groups, and the alignment of key pharmacophore regions with the target [31]. The bond angles and bond lengths (Å) of the three molecules identified as the most suitable have been calculated. The corresponding visuals are provided in **Figures 8** and **Figure 9**. The Mulliken atomic charge is of critical importance in drug design. The partial charge of each atom in a molecule indicates the electron density around that atom and, consequently, its polarity. Especially where covalent bonds are not 100% homogeneous, dipoles, hydrogen bonds, and ionic interactions arise due to these partial charge differences [32,33]. Therefore, the Mulliken atomic charges of the atoms in our ideal molecule were calculated using the Gaussian 09W program [34,35] based on the B3LYP 6-311+G(2d,p) basis set and DFT methods, and the obtained values are indicated on the molecule in **Figure 10**.

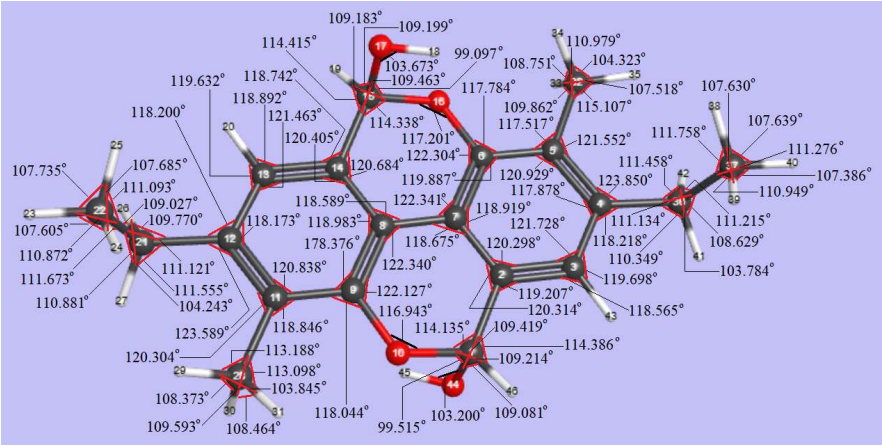

Figure 8. Bond angles between atoms in molecule **(3)**

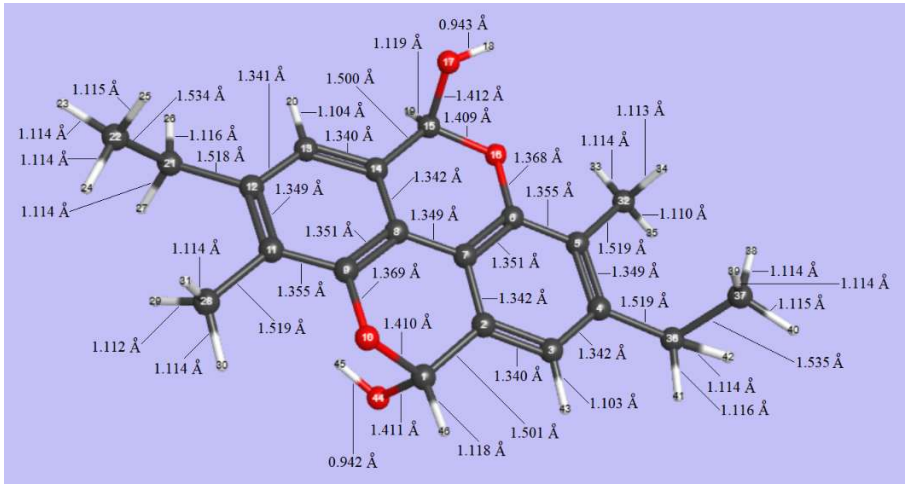

Figure 9. Bond lengths between atoms in molecule **(3)**

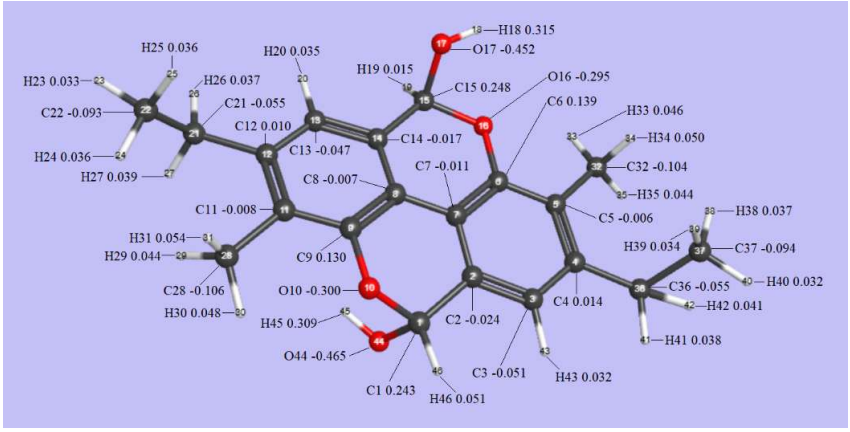

Figure 10. Mulliken atomic charge values of the molecule **(3)**

Quantum mechanical parameters are fundamental calculable reactivity indices that determine a molecule's electronic structure, reactivity potential, stability tendency, electrostatic distribution, polarity, and bonding compatibility [36]. Using the Gaussian 09W program based on the DFT methods on the basis set of B3LYP 6-311+G(2d,p), the some quantum mechanical parameters E_{HOMO} (electron donation tendency, nucleophilic reactivity) and E_{LUMO} (electron acceptance tendency/electrophilic reactivity), chemical potential (μ, reactivity/equilibrium), electron affinity (EA), global softness (S, chemical interaction sensitivity), global hardness (η, electronic stability/polarization tendency), ionization potential (IP, resistance to electron loss), electrophilicity (ω, potential to interact with electron-rich regions of the target), self-Consistent Field (SCF, conformational stability) energy, dipole moment (solubility/ membrane penetration/ target binding), and molecular electrostatic potential (MEP, binding site/H-bonds/ionic interaction prediction) were calculated for molecule **(3)**, which I defined as the ideal molecule. The obtained values are presented in **Table 2**. The figures related to E_{HOMO}/E_{LUMO} and MEP are given in **Figure 11** and **Figure 12**.

Table 2. Some quantum mechanical paramaters calculated for molecule **(3)**

Paramater	Result
E_{LUMO} (a.u)	0.255
E_{HOMO} (a.u)	-0.337
ΔE (E_{LUMO}-E_{HOMO}, a.u)	0.632
IP (ionization potential, a.u)	0.377
EA (electron affinity, a.u)	-0.255
μ (chemical potential, a.u)	0.061
η (global hardness, a.u)	0.316
S (global softness, a.u)	1.582
ω (electrophilicity, a.u)	0.005887658
SCF (self-consistent field, a.u)	-70.301
Dipole moment (debye)	1.669

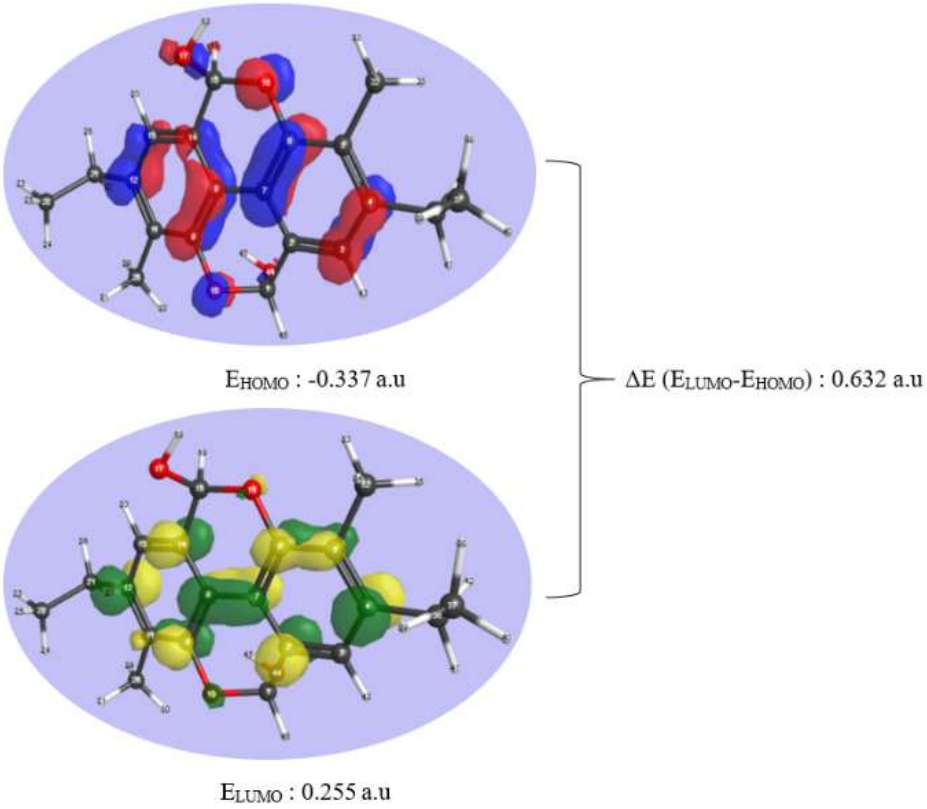

Figure 11. Visual representation of E_{HOMO} and E_{LUMO} values for molecule **(3)**

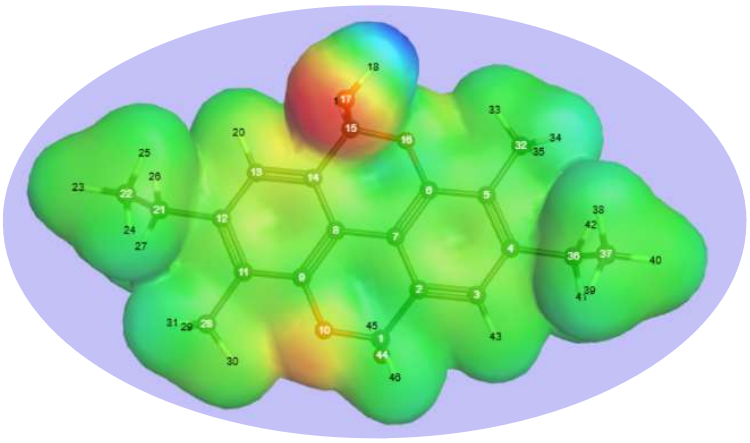

Figure 12. Molecular electrostatic potential (MEP) for molecule **(3)**

When examining the MEP shown in Figure 11, it can be seen that the molecule has a mixed structure that can act as both an H-bond donor and acceptor. Carbonyl or hydroxyl regions can generally interact with polar amino acids (Ser, Thr, Tyr, Asn, and Gln) in enzyme active sites. Aromatic cores, on the other hand, have been determined to have a structure that can stabilize π–π stacking or hydrogen bond networks.

The "Molecular Dynamics Simulation" of the ideal molecule was performed using a web-based server called "iMODS (Internal Coordinate Normal Mode Analysis Server) [27]" following a thorough literature review [37-42]. This method quickly analyzes the

conformational flexibility and internal movements of in silico protein–ligand complexes. Classical MD simulation iteratively solves the motion over time using atom-atom force fields. iMODS, on the other hand, performs Normal Mode Analysis (NMA) and calculates the lowest-energy vibration modes to predict the molecule's natural movement tendencies.Deformability provides relatively strong information about structural flexibility in molecular dynamics simulation. Deformability calculations are typically obtained from matrix-based solutions such as the Hessian matrix and B-factor analysis [43]. The resulting values are for comparison purposes and do not provide absolute position information. First, a deformability graph was plotted against the atom index. The resulting graph is shown in **Figure 13**.

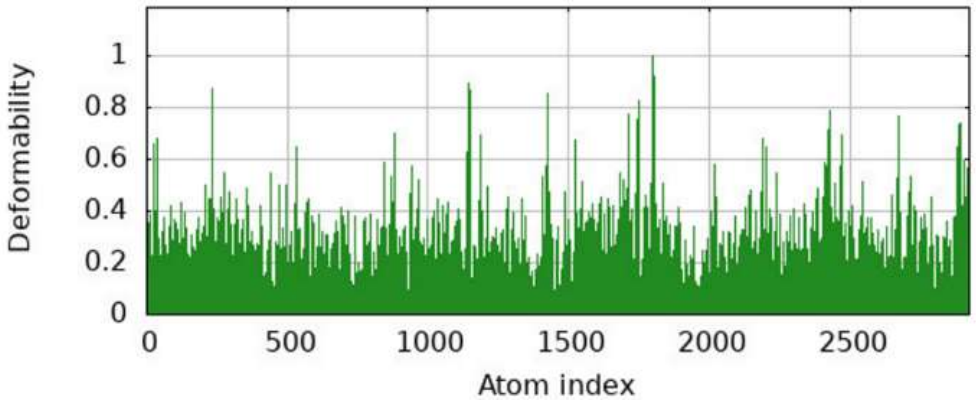

Figure 13. Deformability graph against atom index for Molecule **(3)** in molecular dynamics simulation

Deformability values generally remain low, around 0.2–0.5. This indicates that the structure is generally stable and rigid. However, peak values (0.6–0.9) are observed at certain points (around ~1000, ~1800, and ~2600). These regions are likely loop regions or more mobile segments on the surface.

In molecular dynamics (MD) simulations, the B factor, also known as the Debye-Waller factor or temperature factor, is a parameter that quantitatively expresses the thermal mobility (vibration) of atoms [44]. Although it is generally associated with crystalline structures, it is also used in MD simulations to measure atomic fluctuations. This term, frequently used in molecular dynamics (MD) simulations and statistical physics, describes the dynamic changes in a system over time. The B factor indicates how much an atom deviates from its average position (i.e., how much it vibrates or moves) [45]. Secondly, a Bfactor graph was plotted against the atom index. The resulting graph is shown in **Figure 14**.

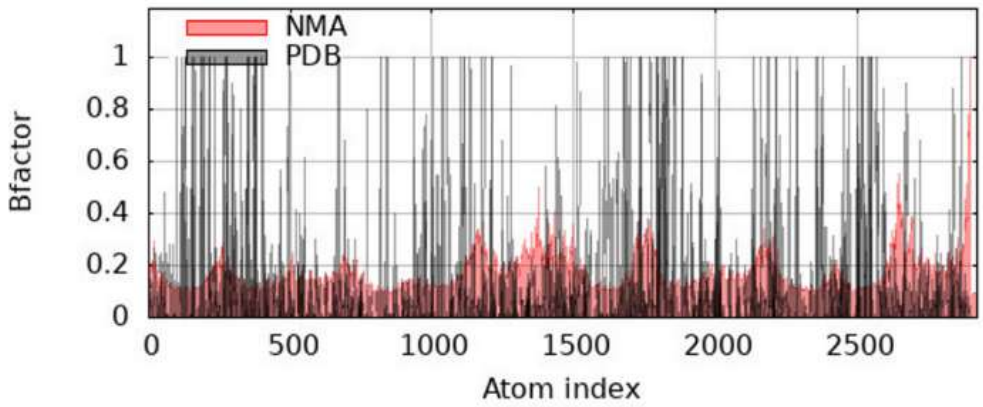

Figure 14. Bfactor graph against atom index for Molecule **(3)** in molecular dynamics simulation

When examining the graph in **Figure 14**, the NMA and experimental B factors generally follow a similar trend. This shows that the NMA model successfully predicts the flexibility profile. However, in some regions (e.g., between 500–700 and 1600–1800), the NMA estimate is lower than the experimental data. NMA is quite successful in predicting the large-scale collective movements of the structure, but the detailed accuracy decreases in regions with high fluctuations (especially at the ends and surfaces).

The Dynamic Cross-Correlation Matrix (DCCM) graph is typically used to visualize correlations between residues within a protein as a result of molecular dynamics simulations [46]. In other words, it shows how amino acids in different regions of a protein move relative to each other. The DCCM answers questions such as which regions move together and which move oppositely [47]. In our study, the Dynamic Cross-Correlation Matrix graph was created as the third stage of the simulation. The resulting graph is given in **Figure 15**.

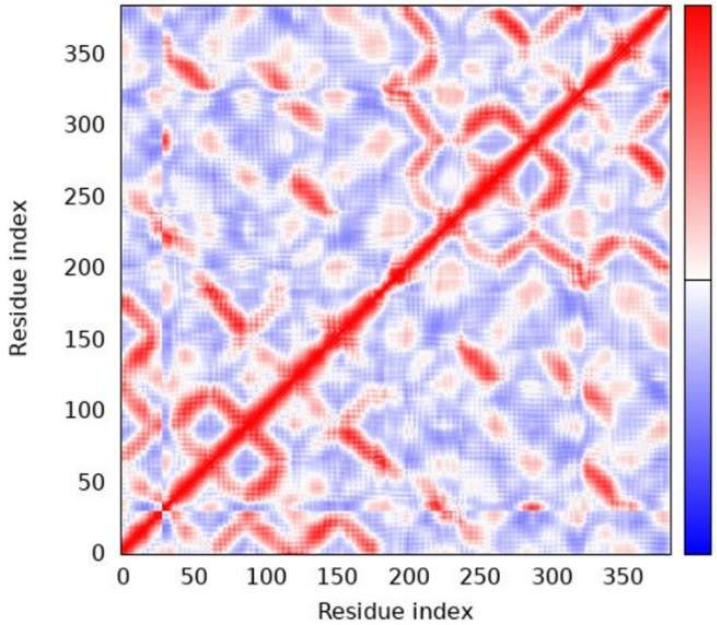

Figure 15. Dynamic Cross-Correlation Matrix graph for Molecule (3) in molecular dynamics simulation

When examining the graph shown in **Figure 15**, it can be seen that some residue groups move collectively. Functional areas such as ligand binding sites, active sites, and substrate recognition sites are generally seen to move together. Negative correlations in terms of structural flexibility and compensation indicate that the two regions move in opposite directions. One region shows strong correlations with a large number of other regions. Ligand-binding regions are generally observed to have high correlations with surrounding residues.

Finally, an atomic contact map was created in molecular dynamics simulations. This map visualizes which atom pairs in the protein structure remain within a certain distance threshold and how long these contacts are maintained. The contact map is a powerful tool used to visualize contact regions and the dynamic stability of these contacts, particularly in protein–protein, protein–ligand, or macromolecule–macromolecule interaction analyses [48]. The contact map obtained for Molecule **(3)** is shown in **Figure 16**.

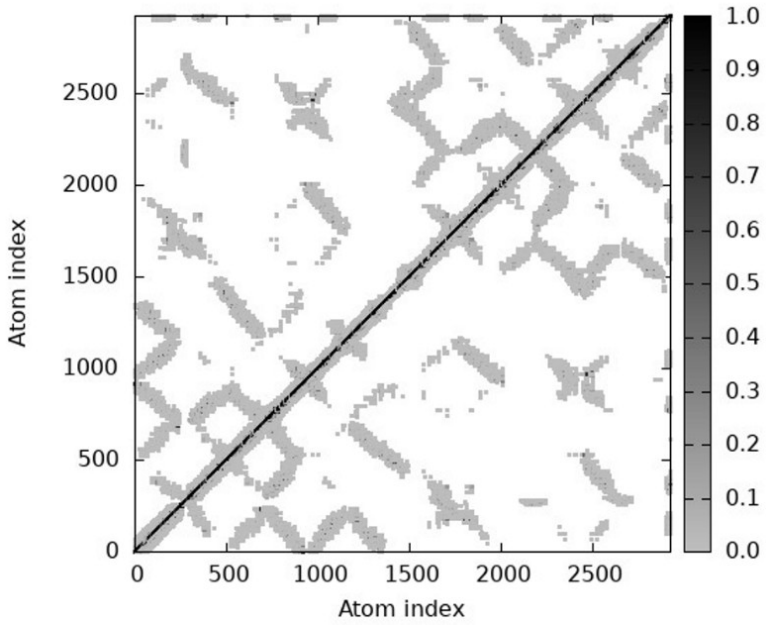

Figure 16. Atomic contact map graph for Molecule **(3)** in molecular dynamics simulation

When examining the contact map shown in **Figure 16**, high contact durations (0.8–1.0) indicate that the folded form of the protein was maintained throughout the simulation. Stable contacts away from the diagonal support that the core regions or subunits of the protein remained compact. Scattered gray areas indicate that loops or flexible regions retained their natural mobility. In conclusion, the simulation indicates that a compact, natural, and stable structure was maintained, with distinct flexible loop regions retaining their mobility and the primary folding regions remaining intact.

I presented a synthesis mechanism for how to synthesize molecule **(3)**, which I

concluded could be evaluated as an active pharmaceutical ingredient. For this purpose, I used the retrosynthesis prediction feature on the ASKCOS [49] to provide a synthesis flow diagram showing how this molecule, which had not been synthesized before, could be synthesized (**Scheme 1**). Theoretically, the synthesis of this molecule can be carried out in a laboratory environment using the synthesis route I have proposed.

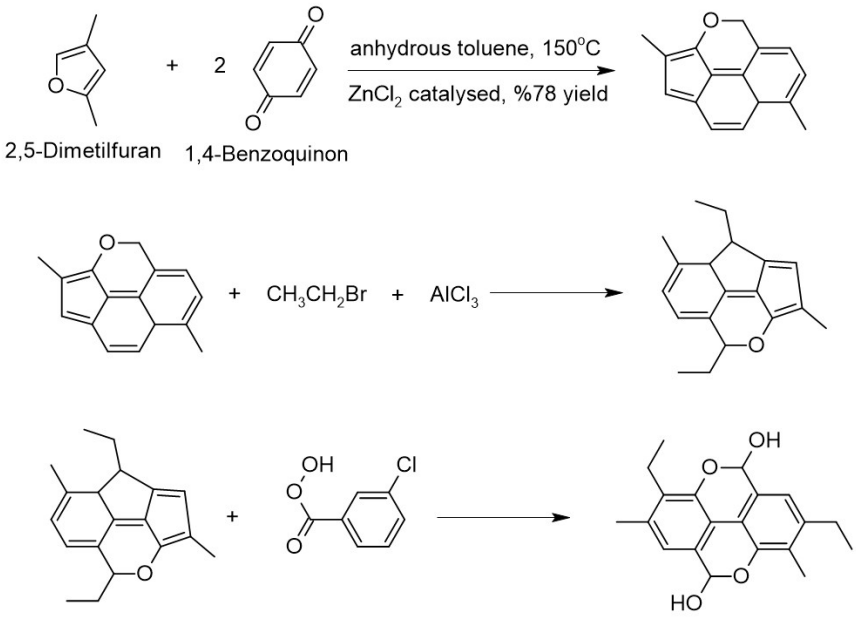

Scheme 1. Retrosynthesis prediction for molecule (3)

Conclusion

In this study, the potential of five different 5,10-dihydrochromeno[5,4,3-cde] chromene-5,10-diol derivative compounds, which have not been synthesized before and are not recorded in the literature, was investigated for use in the treatment of Huntington's disease. Based on the results obtained from the BOILED-Egg graph, bioavailability radars, and molecular docking, it was concluded that molecule **(3)** (2,7-diethyl-3,8-dimethyl-5,10-dihydrochromeno [5,4,3-cde]chromene-5,10-diol) could be used in the treatment of the relevant disease. In line with this result, aromaticity, interpolated charge, H-bonds, hydrophobicity, ionizability, and SAS (solvent accessible surface area) were examined to fully elucidate the structure of the appropriate molecule. Subsequently, the values of bond angles, bond lengths (Å), Mulliken atomic charge (a.u), and some quantum mechanical parameters were calculated. The molecular electrostatic potential was examined, and molecular dynamics simulation was performed for the relevant molecule. Finally, a synthesis flow diagram was created for the synthesis of the relevant molecule in a laboratory environment. In addition to this study, the next step will be to calculate the ADMET and biological

activity values of these molecules, which will provide an opportunity to better understand the ideal molecule.

Acknowledgment

I would like to express my sincere gratitude to Recep Tayyip Erdogan University for their support throughout this research project.

References

[1] Roos R. Huntington's disease: a clinical review. Orphanet Journal of Rare Diseases 2010;5(1):1–8.

[2] McAllister B, Gusella J, Landwehrmeyer G, Lee J, MacDonald M, Orth M, Rosser A, Williams N, Holmans P, Jones L, Massey T. The timing and impact of psychiatric, cognitive and motor abnormalities in Huntington's disease. Neurology 2021;96(19):E2395–E2406.

[3] Pizzorni N, Pirola F, Ciammola A, Schindler A. Management of dysphagia in Huntington's disease: a descriptive review. Neurological Sciences 2020;41(6):1405-1417.

[4] Bachoud-Lévi A, Ferreira J, Massart R, Youssov K, Rosser A, Busse M, Craufurd D, Reilmann R, De Michele G, Rae D, Squitieri F, Seppi K, Perrine C, Scherer-Gagou C, Audrey O, Verny C, Burgunder J. International Guidelines for the Treatment of Huntington's Disease. Frontiers in Neurology 2019;10:1–18.

[5] De Tommaso M, Serpino C, Sciruicchio V. Management of Huntington's disease: role of tetrabenazine. Therapeutics and Clinical Risk Management 2011;7:123.

[6] Rodrigues F, Duarte G, Costa J, Ferreira J, Wild E. Tetrabenazine Versus Deutetrabenazine for Huntington's Disease: Twins or Distant Cousins? Movement Disorders Clinical Practice 2017;4(4):582-585.

[7] Paleacu D, Anca M, Giladi N. Olanzapine in Huntington's disease. Acta Neurologica Scandinavica 2002;105(6):441-444.

[8] Parsa M, Szigethy E, Voci J, Meltzer H. Risperidone in Treatment of Choreoathetosis of Huntington's Disease. Journal of Clinical Psychopharmacology 1997;17(2):134-135.

[9] Ugbe F, Edache E, Adeniji S, Arthur D, Ajala A, Adawara S, Ejeh S, Ibrahim Z. Computational evaluation of the inhibitory potential of some urea, thiourea, and selenourea derivatives of diselenides against leishmaniasis: 2D-QSAR, pharmacokinetics, molecular docking, and molecular dynamics simulation. Journal of Molecular Structure 2024;1302:137473.

[10] Mkhayar K, Elkhattabi K, Elkhalabi R, Haloui R, Daoui O, Edache EI, Elkhattabi S. Evaluation of dimedone-derived compounds as inhibitors against human colon cancer: Insights from 2D-QSAR, ADMET prediction, Osiris, Molinspiration, and molecular modeling. Chinese Journal of Analytical Chemistry 2023;51(11):100330.

[11] Ugbe F, Edache E, Ayuba A, Ibrahim M, Umar A, Adeniji S, Abdalla M, Al-Megrin W, Eltayeb L, Thagfan F, Albutti A, Al-Shouli S. Cheminformatic evaluation of the multi-protein binding potential of some diselenide derivatives: A plausible drug discovery approach for leishmaniasis. Discover Chemistry 2024;1(1):25.

[12] Edache E, Ugbe F, Dawi H, Adedayo A, Umar A, Albutti A. Pharmacophore modeling, 2D-QSAR, drug likeness and toxicity prediction of 2-aziridinyl- and 2,3-bis(aziridinyl)-1,4-naphthoquinonyl sulfonate and acylate derivatives as multifunctional agents for the treatment of malaria parasite, Plasmodium falciparum. NAM Journal 2025;1:100019.

[13] Lafridi H, Almalki F, Ben Hadda T, Berredjem M, Kawsar S, Alqahtani A, Esharkawy E, Lakhrissi B, Zgou H. In silico evaluation of molecular interactions between macrocyclic inhibitors with the HCV NS3 protease. Docking and identification of antiviral

pharmacophore site. Journal of Biomolecular Structure and Dynamics 2022;41(6):2260-2273.

[14] Kawsar S, Munia N, Saha S, Ozeki Y. In Silico Pharmacokinetics, Molecular Docking and Molecular Dynamics Simulation Studies of Nucleoside Analogs for Drug Discovery- A Mini Review. Mini-Reviews in Medicinal Chemistry 2024;24(11):1070-1088.

[15] Kawsar S, Hosen M, El Bakri Y, Ahmad S, Affi S, Goumri-Said S. In silico approach for potential antimicrobial agents through antiviral, molecular docking, molecular dynamics, pharmacokinetic and bioactivity predictions of galactopyranoside derivatives. Arab Journal of Basic and Applied Sciences 2022;29(1):99-112.

[16] Akter N, Bourougaa L, Ouassaf M, Bhowmic R, Uddin K, Bhat A, Ahmed S, Kawsar S. Molecular docking, ADME-Tox, DFT and molecular dynamics simulation of butyroyl glucopyranoside derivatives against DNA gyrase inhibitors as antimicrobial agents. Journal of Molecular Structure 2024;1307:137930.

[17] Daina A, Michielin O, Zoete V. SwissADME: a free web tool to evaluate pharmacokinetics, drug-likeness and medicinal chemistry friendliness of small molecules. Scientific Reports 2017;7(1):1–13.

[18] Fu L, Shi S, Yi J, Wang N, He Y, Wu Z, Peng J, Deng Y, Wang W, Wu C, Lyu A, Zeng X, Zhao W, Hou T, Cao D. ADMETlab 3.0: an updated comprehensive online ADMET prediction platform enhanced with broader coverage, improved performance, API functionality and decision support. Nucleic Acids Research 2024;52(W1):W422-W431.

[19] Chem3D, version 22.0. PerkinElmer Inc.: Waltham, USA; 2022.

[20] BIOVIA, Dassault Systèmes. Discovery Studio Visualizer, version 2019. Dassault Systèmes: San Diego, USA; 2019.

[21] Eberhardt J, Santos-Martins D, Tillack A, Forli S. AutoDock Vina 1.2.0: New Docking Methods, Expanded Force Field, and Python Bindings. Journal of Chemical Information and Modeling 2021;61(8):3891–3898.

[22] Trott O, Olson A. AutoDock Vina: Improving the speed and accuracy of docking with a new scoring function, efficient optimization, and multithreading. Journal of Computational Chemistry 2009;31(2):455-461.

[23] Kumar M, Rathore R. RamPlot: a webserver to draw 2D, 3D and assorted Ramachandran (φ, ψ) maps. Journal of Applied Crystallography 2025;58(2):630-636.

[24] Zhao C, Wu H, Liu H, Dong H, Niu M, Shi K, Wang F. Discovery of novel dual-targeting inhibitors against PLK1-PBD and PLK4-PB3: structure-guided pharmacophore modelling, virtual screening, molecular docking, molecular dynamics simulation, and biological evaluation. Journal of Enzyme Inhibition and Medicinal Chemistry 2025;40(1):2522810.

[25] Chang T, Chang R, Tseng H. Molecular dynamics simulation of slit rheometer for predicting shear thinning of short polyethylene chains. Physics of Fluids 2024;36(9):9–23.

[26] Li M, Hu B, Hou W, Han G, Song X, Lei X. Thermodynamic mechanism based on thermoplastic epoxy resin/polyethylene glycol composites: An experimental and molecular dynamics simulation study. Journal of Molecular Structure 2025;1345:143191.

[27] López-Blanco J, Aliaga J, Quintana-Ortí E, Chacón P. iMODS: internal coordinates normal mode analysis server. Nucleic Acids Research 2014;42(W1):W271-W276.

[28] Kmiecik S, Kouza M, Badaczewska-Dawid A, Kloczkowski A, Kolinski A. Modeling of Protein Structural Flexibility and Large-Scale Dynamics: Coarse-grained Simulations and Elastic Network Models. International Journal of Molecular Sciences 2018;19(11):3496.

[29] Imberty A, Hardman K, Carver J, Perez S. Molecular modelling of protein-carbohydrate interactions. Docking of monosaccharides in the binding

site of concanavalin A. Glycobiology 1991;1(6):631-642.

[30] Anderson A. The Process of Structure-Based Drug Design. Chemistry & Biology 2003;10(9):787-797.

[31] Alotaiq N, Dermawan D. Computational Investigation of Montelukast and Its Structural Derivatives for Binding Affinity to Dopaminergic and Serotonergic Receptors: Insights from a Comprehensive Molecular Simulation. Pharmaceuticals 2025;18(4):559.

[32] Chimarro-Contreras A, Lopez-Revelo Y, Cardenas-Gamboa J, Terencio T. Insights into the Effect of Charges on Hydrogen Bonds. International Journal of Molecular Sciences 2024;25(3):1613.

[33] Xie Q, Horsfield A. Coordinate-Free and Low-Order Scaling Machine Learning Model for Atomic Partial Charge Prediction for Any Size of Molecules. Journal of Chemical Information and Modeling 2024;64(11):4419-4425.

[34] Frisch MJ, Trucks GW, Schlegel HB, Scuseria GE, Robb MA, Cheeseman JR, Scalmani G, Barone V, Mennucci B, Petersson GA, Nakatsuji H, Caricato M, Li X, Hratchian HP, Izmaylov AF, Bloino J, Zheng G, Sonnenberg JL, Hada M, Ehara M, Toyota K, Fukuda R, Hasegawa J, Ishida M, Nakajima T, Honda Y, Kitao O, Nakai H, Vreven T, Montgomery JA Jr, Peralta JE, Ogliaro F, Bearpark M, Heyd JJ, Brothers E, Kudin KN, Staroverov VN, Kobayashi R, Normand J, Raghavachari K, Rendell A, Burant JC, Iyengar SS, Tomasi J, Cossi M, Rega N, Millam JM, Klene M, Knox JE, Cross JB, Bakken V, Adamo C, Jaramillo J, Gomperts R, Stratmann RE, Yazyev O, Austin AJ, Cammi R, Pomelli C, Ochterski JW, Martin RL, Morokuma K, Zakrzewski VG, Voth GA, Salvador P, Dannenberg JJ, Dapprich S, Daniels AD, Farkas Ö, Foresman JB, Ortiz JV, Cioslowski J, Fox DJ. Gaussian 09, Revision B.01. Gaussian Inc.: Wallingford, USA, 2009.

[35] Foresman JB, Frisch AE. Exploring chemistry with electronic structure methods. 2nd ed. Gaussian Inc.: Wallingford, USA; 1996.

[36] Nalewajski R. Understanding Electronic Structure and Chemical Reactivity: Quantum-Information Perspective. Applied Sciences 2019;9(6):1262.

[37] Edache E, Uzairu A, Mamza P, Shallangwa G, Ibrahim M. Design of some potent non-toxic Autoimmune disorder inhibitors based on 2D-QSAR, CoMFA, molecular docking, and molecular dynamics investigations. Intelligent Pharmacy 2024;2(5):688-706.

[38] Ugbe F, Edache E, Adeniji S, Arthur D, Ajala A, Adawara S, Ejeh S, Ibrahim Z. Computational evaluation of the inhibitory potential of some urea, thiourea, and selenourea derivatives of diselenides against leishmaniasis: 2D-QSAR, pharmacokinetics, molecular docking, and molecular dynamics simulation. Journal of Molecular Structure 2024;1302:137473.

[39] Edache EI, Uzairu A, Mamza PA, Shallangwa GA. Investigation of salicylidene acylhydrazides derivatives: Molecular Docking, ADMET, and Molecular Dynamic Simulations were used in conjunction towards the design of new Yersinia pseudotuberculosis inhibitors. Turkish Computational and Theoretical Chemistry 2022;6(1):9-30.

[40] Ugbe F, Ayuba A, Edache E, Jibrin A, Amusan O. Evaluation of the anti-leishmanial potential of some prominent lead compounds against pyridoxal kinase in complex with adenosine diphosphate and pyridoxine: a comparative study. Acta Scientifica Malaysia 2024;8(2):61-73.

[41] Ugbe F, Shallangwa G, Uzairu A, Abdulkadir I, Edache E, Al-Megrin W, Al-Shouli S, Wang Y, Abdalla M. Cheminformatics-based discovery of new organoselenium compounds with potential for the treatment of cutaneous and visceral leishmaniasis. Journal of Biomolecular Structure and Dynamics 2023;42(24):13830-13853.

[42] Edache E, Uzairu A, Mamza P, Shallangwa G. 2D-QSAR, Docking, Molecular Dynamics Simulations with the MM/GBSA Approaches against Graves' Disease and PTPN22. Borneo Journal of Pharmacy 2023;6(3):229-248.

[43] González-Paz L, Hurtado-León M, Lossada C, Fernández-Materán F, Vera-Villalobos J, Loroño M, Paz J, Jeffreys L, Alvarado Y. Structural deformability induced in proteins of potential interest associated with COVID-19 by binding of homologues present in ivermectin: Comparative study based in elastic networks models. Journal of Molecular Liquids 2021;340:117284.

[44] Pang Y. Use of multiple picosecond high-mass molecular dynamics simulations to predict crystallographic B-factors of folded globular proteins. Heliyon 2016;2(9):e00161.

[45] Xu G, Yang Y, Lv Y, Luo Z, Wang Q, Ma J. OPUS-BFactor: Predicting protein B-factor with sequence and structure information. Molecules 2025;30(12):2570.

[46] Kasahara K, Fukuda I, Nakamura H. A Novel Approach of Dynamic Cross Correlation Analysis on Molecular Dynamics Simulations and Its Application to Ets1 Dimer–DNA Complex. PLoS ONE 2014;9(11):e112419.

[47] Arnold G, Ornstein R. Molecular dynamics study of time-correlated protein domain motions and molecular flexibility: cytochrome P450BM-3. Biophysical Journal 1997;73(3):1147-1159.

[48] Abdel-Azeim S, Chermak E, Vangone A, Oliva R, Cavallo L. MDcons: Intermolecular contact maps as a tool to analyze the interface of protein complexes from molecular dynamics trajectories. BMC Bioinformatics 2014;15(S5):S1.

[49] Tu Z, Choure S, Fong M, Roh J, Levin I, Yu K, Joung J, Morgan N, Li S, Sun X, Lin H, Murnin M, Liles J, Struble T, Fortunato M, Liu M, Green W, Jensen K, Coley C. ASKCOS: Open-Source, Data-Driven Synthesis Planning. Accounts of Chemical Research 2025;58(11):1764-1775.